9

Research article

Youxian Shan, Zhongfu Li, Banxian Ruan, Jiaqi Zhu, Yuanjiang Xiang and Xiaoyu Dai*

Two-dimensional Bi₂S₃-based all-optical photonic devices with strong nonlinearity due to spatial self-phase modulation

https://doi.org/10.1515/nanoph-2019-0231 Received July 30, 2019; revised October 12, 2019; accepted October 14, 2019

Abstract: Bismuth sulfide (Bi₂S₃) is a binary chalcogenide semiconductor compound that has received much attention in optoelectronic devices because of its stratified structure. In this work we showed that the twodimensional (2D) Bi₂S₂ shows strong nonlinearity using spatial self-phase modulation and that the all-optical photonic devices, e.g. the all-optical switches and all-optical diodes, have been demonstrated experimentally by observing the nonlinear behavior of the diffraction rings. In addition, an all-optical diode is designed in this work using combined structure with 2D Bi₂S₂/SnS₂ nanosheet by taking advantage of the reverse saturated absorption of 2D SnS₂ and saturated absorption of 2D Bi₂S₂. Nonreciprocal light propagation has been achieved with different incident wavelength and a variety of incident intensities. Those characteristics make 2D Bi₂S₂ a potential candidate for the next generation nonreciprocal all-optical device.

Keywords: spatial self-phase modulation; all-optical diode; all-optical switch.

1 Introduction

Bismuth sulfide (Bi₂S₃) is a binary chalcogenide semiconductor compound belonging to the V–VI group with

*Corresponding author: Xiaoyu Dai, International Collaborative Laboratory of 2D Materials for Optoelectronic Science and Technology of Ministry of Education, Institute of Microscale Optoelectronics (IMO), Shenzhen University, Shenzhen 518060, China, e-mail: xiaoyudai@126.com

Youxian Shan, Zhongfu Li, Banxian Ruan, Jiaqi Zhu and Yuanjiang Xiang: International Collaborative Laboratory of 2D Materials for Optoelectronic Science and Technology of Ministry of Education, Institute of Microscale Optoelectronics (IMO), Shenzhen University, Shenzhen 518060, China. https://orcid.org/0000-0002-7225-5411 (Y. Xiang)

a bandgap of 1.3 eV [1]. Thair et al. used aerosol-assisted chemical vapor deposition to synthesize Bi₂S₂ nanotube films with high photosensitivity and light response signals under illumination [2]. Bi₃S₃, nanosheet is considered as an excellent absorbing material [3] with an absorption coefficient of $\alpha \approx 10^5$ cm⁻¹, and it has a wide range of applications in the field of nonlinear optics. Compared with other semiconductor materials, Bi₂S₂ has received much attention because of its stratified structure [4–6], which makes Bi₃S₃ a good candidate as photovoltaic devices, photoconductors, catalysis, and electrochemistry [7–11]. Conversely, SnS, is a IV–VI compound semiconductor belonging to the hexagonal crystal system (lattice constant a = 0.365 nm, b = 0.365 nm, and c = 0.589 nm) with a bandgap of 2.6 eV [12]. With the strong optical absorption capability ($\alpha > 2 \times 10^4 \, \text{cm}^{-1}$) [13], SnS, has been used as thin films for solar cell production. Additionally, the ultra-wideband and reverse saturated absorption (RSA) characteristic of SnS, have made it a proper material to design an all-optical diode device combined with other saturated absorption two-dimensional (2D) materials [12].

Spatial self-phase modulation (SSPM) is an effective way to study the nonlinear optical responses of a 2D material [14, 15] using diffraction rings [16]. Compared with the Z-scan technique by self-focusing or self-defocusing [17], the SSPM solution is more straightforward and easier to implement. By means of SSPM, the nonlinear coefficient of some 2D materials have been successfully measured, that is, graphene $(n_2 \approx 10^{-5} \text{ cm}^2 \text{ W}^{-1})$ [18], MoS_2 ($n_2 \approx 10^{-7}$ cm² W⁻¹), WS_2 ($n_2 \approx 10^{-7}$ cm² W⁻¹) [19], and black phosphorus $(n_2 \approx 10^{-5} \text{ cm}^2 \text{ W}^{-1})$ [20]. In this work, we obtained the nonlinear refractive index of Bi₃S₃ at different wavelengths using SSPM: $n_2 = 3.34 \times 10^{-5}$ cm² W⁻¹ with $\lambda = 457$ nm, $n_2 = 1.26 \times 10^{-6}$ cm² W⁻¹ with $\lambda = 532$ nm, and $n_3 = 1.62 \times 10^{-7}$ cm² W⁻¹ with $\lambda = 671$ nm. By taking advantage of strong nonlinearity and the diffraction effect of 2D Bi₂S₂, an all-optical switching device has been designed based on the monochromatic light, which does not have time delay. The proposed switch has shown a faster optical

response compared with other all-optical switches based on the cross-phase modulation [21–26].

Furthermore, it is known that diodes play an important role in electronic devices and systems, because of its unilateral conductivity characteristic. When the applied reverse voltage exceeds the threshold, the diode will breakdown and conduct a huge amount of current [27, 28]. In this paper, we also design a novel all-optical diode with the combined structure of 2D Bi₂S₃ and SnS₂. It is shown that when the laser beam passes the combined structure from the positive direction (Bi₂S₂/SnS₂), the diffraction rings are excited with a normal pattern, which can be considered as an "ON" state. However, if the laser beam passes the combined structure from the reverse direction (SnS₂/Bi₂S₂), no diffraction rings will be excited, representing the "OFF" state [29, 30].

2 Characterization and analysis of sample

Figure 1 shows the typical characterizations of the asprepared Bi₂S₂ nanosheets fabricated by a liquid phase exfoliation method. According to the TEM images shown in Figure 1A, Bi₂S₃ nanosheets are successfully exfoliated with a lateral size ranging from 80 to 210 nm. The HRTEM images show clear lattice fringes of 0.27 and 0.31 nm (Figure 1B), which can be assigned to the lattice spacing in the (221) and (211) planes of Bi₂S₂, respectively [31, 32]. Moreover, a selected area electron diffraction (SAED) pattern (insert in Figure 1B) confirms that the crystal features of the Bi₂S₂ nanosheets keep in good order in liquid phase exfoliation. Additionally, the morphology and thickness of the as-prepared Bi₂S₃ nanosheets were determined by atomic force mircroscopy (Figure 1C-E). Individual thin Bi₂S₂ nanosheets in Figure 1C can be clearly observed, and their thicknesses are measured to be 7.2, 8.4, 13.8, and 15.3 nm (Figure 1E, D, and F), which correspond to 6, 8, 12, and 14 layers, respectively. The estimated thickness of monolayer Bi₂S₃ is 1.11 nm [33]. Ultraviolet-visible (UV-Vis) absorption spectroscopy was employed to characterize the optical response (Figure 1F). It can be clearly observed that the Bi₂S₃ nanosheets have a broadband absorption ranging from 250 to 1000 nm, which shows their great potential to be applied in UV-Vis-near infrared devices. It is worth to be noted that the obtained Bi₂S₂ nanosheets can still be redispersed in NMP (left picture in the Figure 1F left insert) and can be stabilized without any noticeable aggregation for more than 2 weeks at the room temperature. This

is verified by Tyndall effect (right picture in the Figure 1F left insert). During the procedure, the measured bandgap (E_a) energy increases from 1.30 (bulk Bi₂S₃) [34] to 1.68 eV (as-prepared Bi₂S₂ nanosheets; right insert in Figure 1F), which is in accordance with the previous reported results [35, 36]. The Raman spectra of the bulk Bi₂S₃ and Bi₂S₃ nanosheets are shown in Figure 1G. Fixed resonance peaks of bulk Bi_2S_3 are observed at 101.3 (A_g), 168.1 (B_{1g}), 186.2 (A_{σ}), 238.0 (A_{σ}), and 261.7 cm⁻¹ ($B_{1\sigma}$), which agree well with the Raman bands reported by Huang [34] and Trentelman [37]. In addition, it is noticed that Bi₂S₂ nanosheets are red-shifted slightly compared with those of bulk Bi₂S₂ because of the larger free oscillation when fewer layers of Bi₂S₂ are bonded by van der Waals forces. This red-shift phenomenon is similar to the mode change of other 2D materials, such as black phosphorus and its analogue, beta-lead oxide [38, 39].

3 Experiment method and results

3.1 Schematic and experimental diagram of **SSPM**

Figure 2 shows the setup of the SSPM experiments. A laser beam emitted by a laser device passes the neutral optical attenuator, is then focused by a lens, and finally gets through the as-prepared sample (2D Bi₂S₃ dispersions). The optical response of Bi₂S₂ nanosheets resulted in a series of diffraction rings behind the cuvette. The laser device radiates at a fixed power, and the power of the incident light is adjusted using the optical attenuator. The optical lens focused the laser beam to a point, which enhanced the power density and helps excite the nonlinear effect from the 2D Bi₂S₃. The cuvette is used to hold the samples. Figure 1A demonstrates the nonlinear response of the 2D Bi₃S₃ dispersions for $\lambda = 457$ nm; the formation of the diffraction rings takes about 2.2 s. At the beginning, only a green point is formed behind the cuvette, and then the diffraction rings appear and reach the largest aperture after 0.88 s. The internal rings only sustain for a short period and then collapse gradually to half of the ring size at 2.2 s. This procedure shows that the nonlinear optical response of 2D Bi₂S₂ is a dynamic process for the CW laser, and the diffraction ring will eventually remain stable. Figure 1B and C show a similar process as Figure 1A, but the time periods from the formation of the diffraction rings to the collapse are different for each wavelength, and this is due to the different responsivities of 2D Bi₃S₃ dispersions with the various wavelength CW laser.

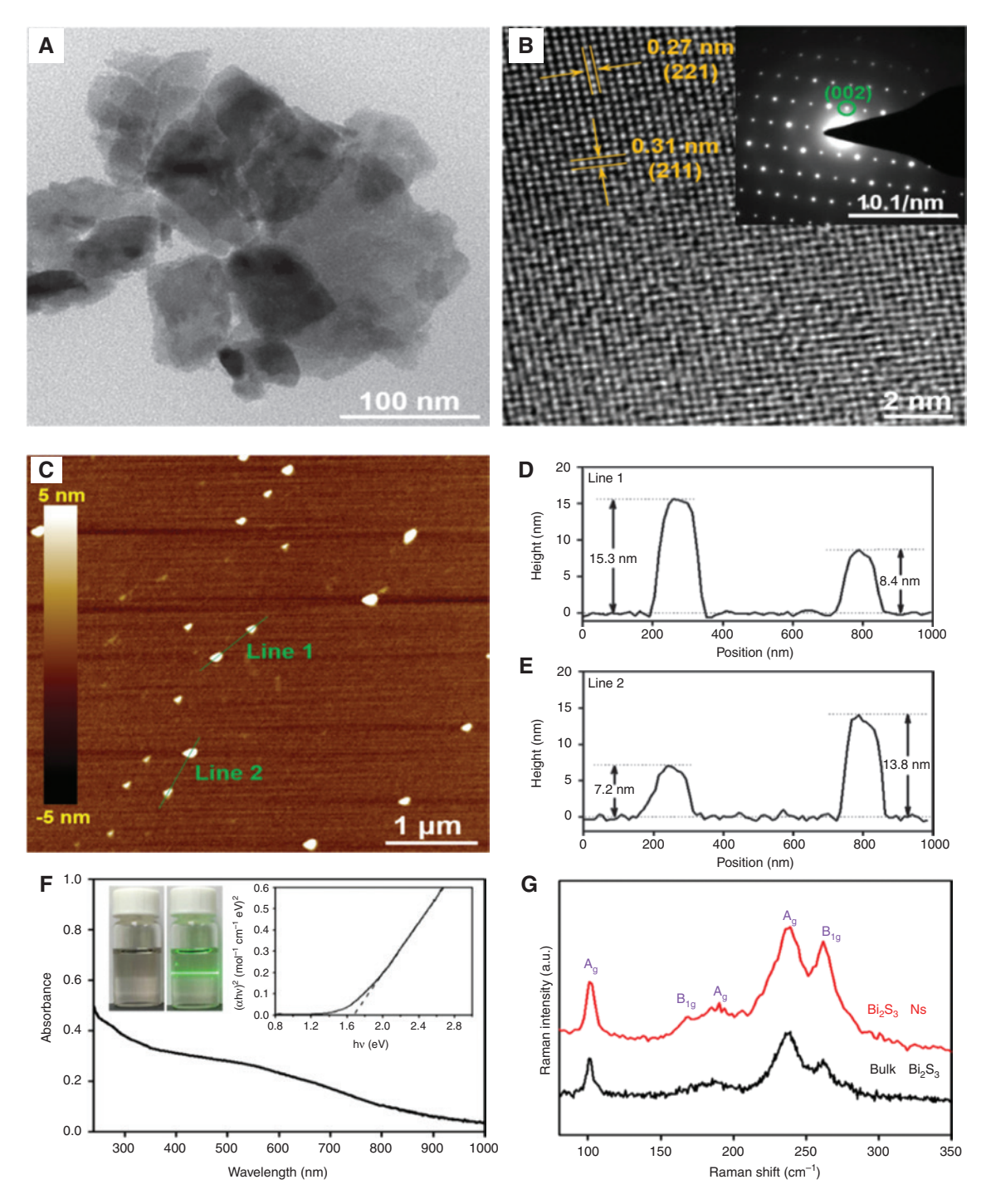


Figure 1: Structural characterization of the as-prepared Bi₂S₃ nanosheets. (A) TEM image of the Bi₂S₃ nanosheets. (B) HRTEM image showing crystalline lattices. Inset: The selected area electron diffraction (SAED) pattern (up right). (C) AFM image of the Bi,S, nanosheets. (D, E) Height profiles along the green lines in (C). (F) UV-Vis absorption spectrum of the Bi,S₃ nanosheets in NMP. Left inset: Photos of the Bi,S₃ nanosheet suspension (left) and the Tyndall effect of the Bi,S₃ nanosheet suspension (right); right insert: Tauc plot for its calculation of the band gap (F_w) energy. (G) Raman spectra of bulk Bi,S₃ and Bi,S₃ nanosheets.

Based on the experiment of SSPM, we set a controlled trial, which is used to verify the relationship between thermal lens effect and optical nonlinearity. In Figure 3A, a chopper is placed behind the attenuator, and

it is able to produce a fixed-frequency laser beam, and its thermal lens effect is weaker than continue wavelength. Figure 3B shows the diffraction ring in modulator frequencies f = 0 Hz, f = 20 Hz, and f = 100 Hz. According to these

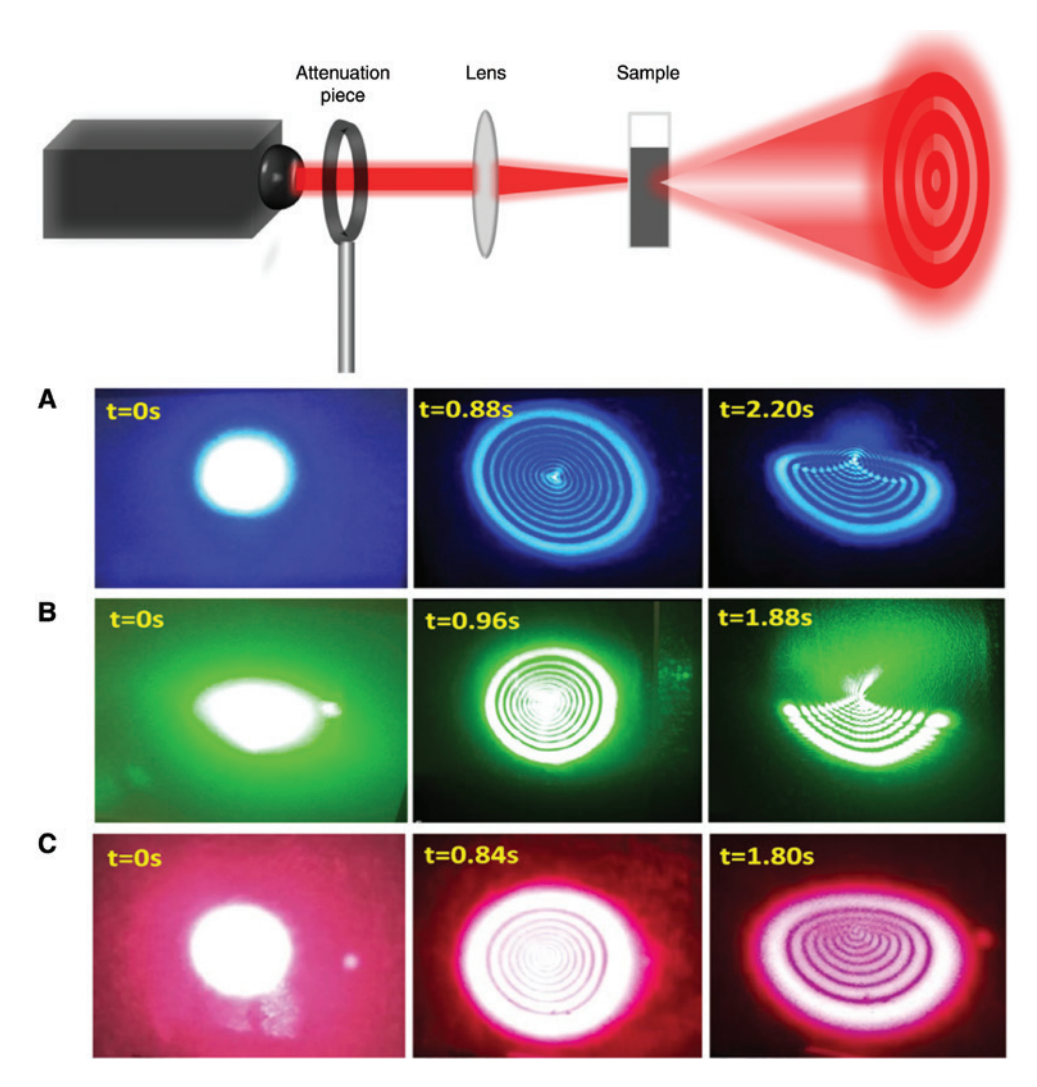


Figure 2: The experimental facility diagram of SSPM. (A), (B), and (C) are the diffraction rings with $\lambda = 457$, 532, and 671 nm, respectively.

results, we can see that the number of diffraction rings in f=20 Hz and f=100 Hz is obviously less than the number of diffraction rings without chopper, which shows that the thermal lens effect plays an important role in optical nonlinearity. Therefore, we believe that both thermal lens effect and Kerr effect lead to the self-phase modulation and the diffraction ring.

3.2 Nonlinear refractive index of Bi₂S₃

From Kerr nonlinearity, we can obtain the equation based on optical nonlinear effect:

$$n = n_0 + n_2 I, \tag{1}$$

where $n_0 = 1.377$ stands for the linear refractive index of isopropanol, n_2 is the nonlinear refractive index of 2D Bi₂S₃

dispersions, and *I* is the incident intensity of laser beam. When the light passes through the 2D Bi₂S₃ dispersions, the nonlinear effect can be excited, and the phase shift can be expressed as follows:

$$\Delta \psi = \frac{2\pi n_0}{\lambda} \int_{0}^{L_{\text{eff}}} n_2 I(r, z) dz, \qquad (2)$$

where L_{eff} is the effective optical thickness of 2D Bi₂S₃ dispersions. In addition, the radial coordinate $r \in (0, \infty)$ represents the distance from the focus point to the farfield, and I(r, z) is the radial intensity distribution of the laser beam. According to the Gaussian beam theory, I (average intensity) is half of the central light intensity I(0, z). In this experiment, the value of *I* can be adjusted. The number of rings (*N*) depends on $\Delta \psi(0) - \Delta \psi(\infty) = 2N\pi$. The expression of L_{off} can be written as follows:

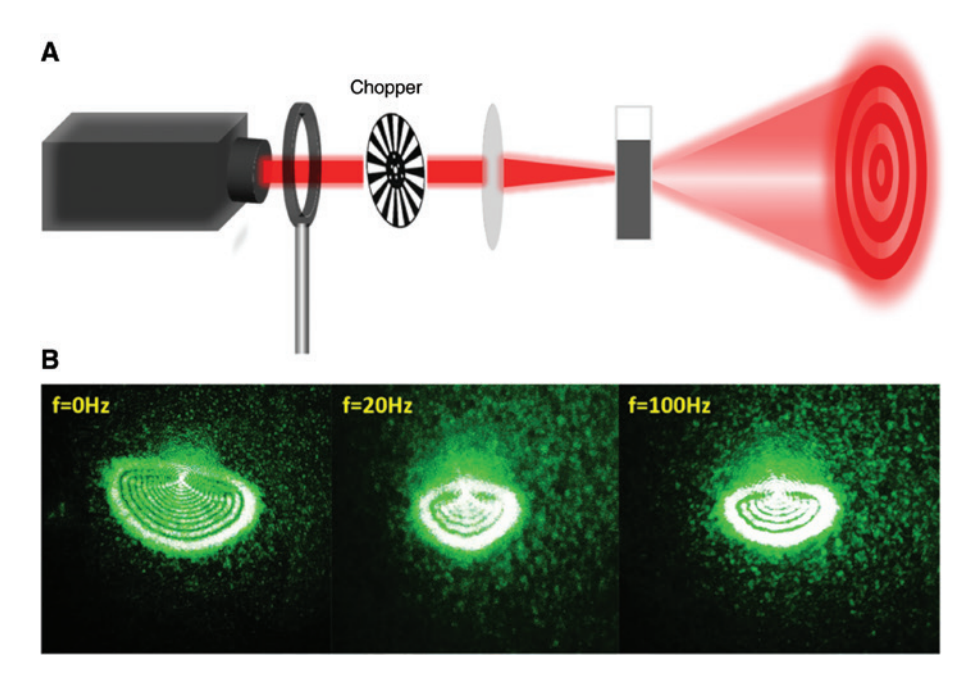


Figure 3: The contrast experiment with different incident intensity. (A) The experimental facility diagram of SSPM and (B) the diffraction ring for the modulator frequencies of f = 0 Hz, f = 20 Hz, f = 100 Hz.

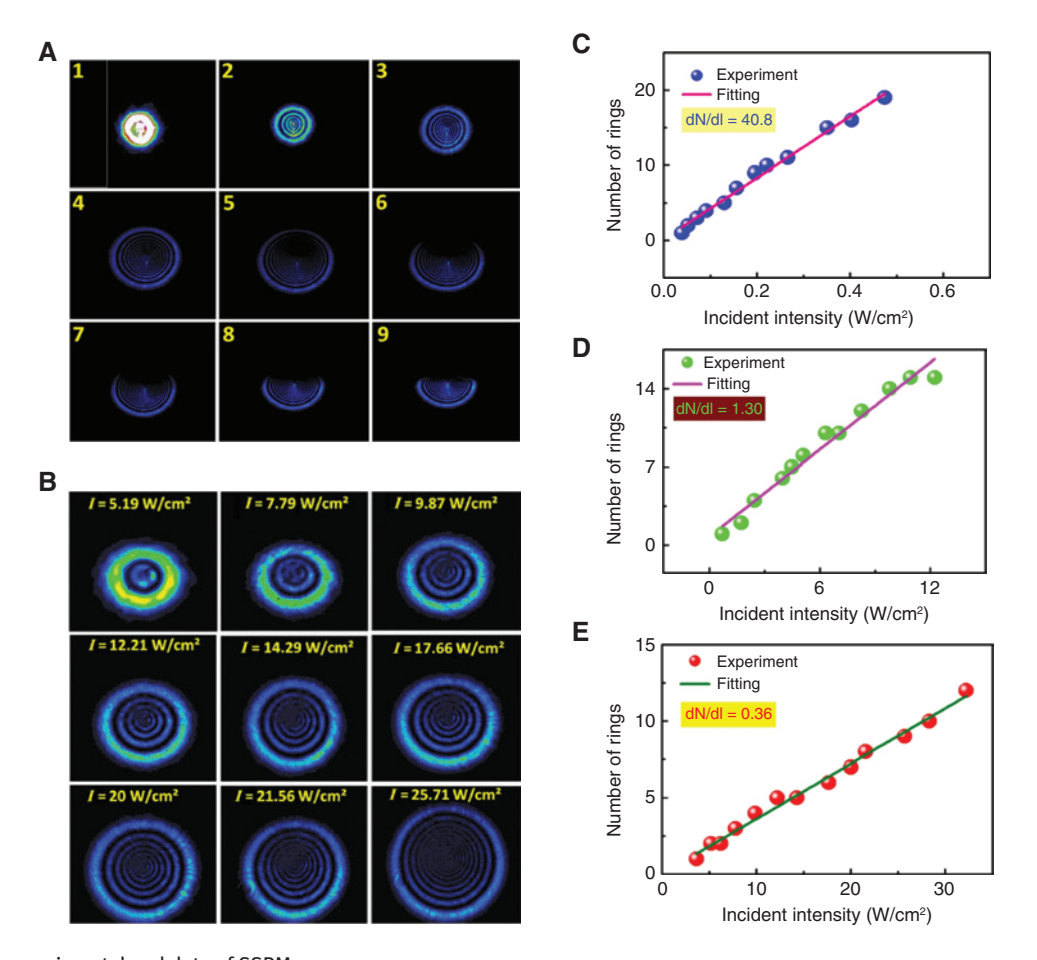


Figure 4: The experimental and data of SSPM. (A) Whole process of diffraction ring, (B) the image of diffraction ring in variety incident intensity, (C), (D), and (E) are the number of the diffraction rings corresponding to the different incident intensity at $\lambda = 457$ nm, $\lambda = 532$ nm, and $\lambda = 671$ nm, respectively.

$$L_{\text{eff}} = \int_{L_1}^{L_2} \left(1 + \frac{z^2}{z_0^2} \right)^{-1} dz = z_0 \arctan |_{L_1}^{L_2}, \left(z_0 = \frac{\pi \omega_0^2}{\lambda} \right), \tag{3}$$

where L_1 and L_2 are distances from the local point to the front and rear surfaces of the quartz cuvette, respectively. Therefore, the cuvette's thickness is $L=L_1-L_2$. ω_0 is the waist radius. In this work, L=1 cm, and the focus of the lens f=10 cm. As a result, the nonlinear index n_2 is given as follows [39]:

$$n_2 = \frac{\lambda}{2n_0 L_{\text{eff}}} \cdot \frac{N}{I} . \tag{4}$$

In this work, three different wavelengths are used to excite the nonlinear effect of ${\rm Bi}_2{\rm S}_3$, and Figure 4 shows the experimental results. Figure 4A illustrates the whole process (1–9) of the diffraction rings formation, from an initial point to the finally collapsed ring at I=25.71 W/cm² with λ =671 nm. Figure 4B shows the diffraction ring formed under various incident intensities when the diffraction rings are fully expanded. It is clear that the number of diffraction rings is closely related to the light intensity. Figure 4C shows the relationship between the number

of rings and incident intensity with $\lambda=457$ nm. In this picture, the blue dots are the experimental data, and the red line is the fitted curve, where the slope $\mathrm{d}N/\mathrm{d}I=40.8$. Similarly, Figure 4D and E show the $\mathrm{d}N/\mathrm{d}I$ curves with $\lambda=532$ nm and $\lambda=671$ nm. According to these results, the nonlinear refractive indexes can be calculated, i.e. $n_2=3.34\times10^{-5}$ cm² W⁻¹ for $\lambda=457$ nm laser, $n_2=1.26\times10^{-6}$ cm² W⁻¹ for $\lambda=532$ nm laser, and $n_2=1.62\times10^{-7}$ cm² W⁻¹ for $\lambda=671$ nm laser.

3.3 All-optical switch based on monochromatic light

All-optical switch based on the cross-phase modulation tends to have optical time delay. In this work, a novel all-optical switching device is proposed based on SSPM of 2D ${\rm Bi}_2{\rm S}_3$ with the monochromatic light, which eliminates the time delay. Figure 5A shows the experimental setup of the all-optical switch with λ = 671 nm laser. In the setup, a red laser beam passes through the attenuator and gets to the beam splitter, which divides the beam into two (pump and reference light). The pump laser beam then excites

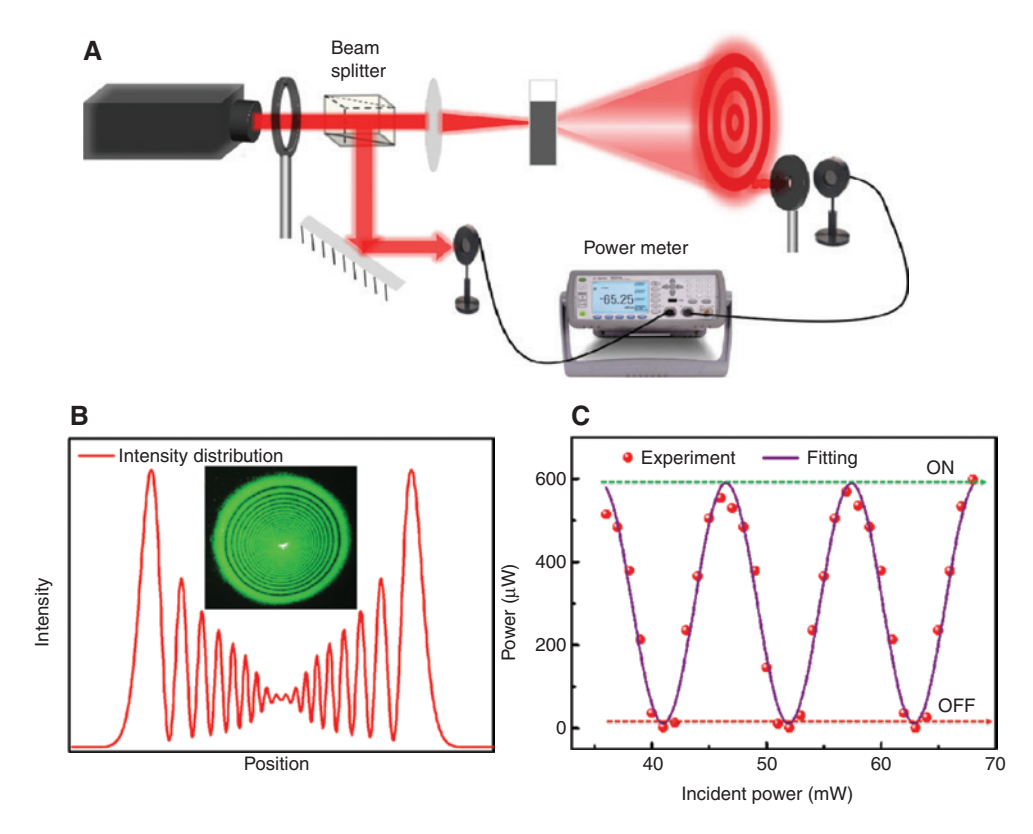


Figure 5: The theory and experiment of all-optical switch.

(A) All-optical switch schematic based on the monochromatic light, (B) theoretical intensity distribution of diffraction rings, and (C) experimental data of all-optical switch function.

the nonlinear effect of the 2D Bi₂S₂ sample, forming a series of diffraction rings. A diaphragm is placed at the outermost diffraction ring to monitor its power. Meanwhile, the power of the reference light is also recorded to compare with the pump light. Figure 5B illustrates the simulation result of the intensity distribution of diffraction rings, and it is found that the intensity reaches the peak value at the outermost ring and declines inward. To verify the simulated results, the intensity of each diffraction ring is measured using a power meter. The measured power distribution agrees with the simulated results. Figure 5C shows the plot of the experimental data of the all-optical switch function using discrete points. Different from the simulation, the incident intensity is adjusted using an attenuator to tune the position of the diffraction. During the procedure, the position of the aperture varies constantly between the dark and bright ring. When the aperture locates at the bright ring, the device is "ON"; in contrast, the dark ring stands for "OFF." As a result, the all-optical switch function has been realized.

3.4 All-optical diode based on Bi₂S₃/SnS₃ nanosheets

Figure 6A shows the physical process of SSPM, where different lasers ($\lambda = 457$, 532, and 671 nm) are used to excite the nonlinear optical responses of 2D Bi₂S₃. Because of the narrow bandgap of Bi₂S₃ (1.3 eV), all three laser beams are able to pump the photon from the valence band to the conduction band and generate the diffraction rings. However, SnS, has a bandgap of 2.6 eV, which requires more energy to pump photon. As depicted in Figure 6B, only the blue laser beam can excite the nonlinear effect and form a series of diffraction rings. Figure 6C illustrates the all-optical diode with a positive propagation of light. The laser beam first passes through the Bi,S,, forming the diffraction ring, and then passes the SnS,, with a darker ring due to the reduced power. The response with a reverse propagation of light is shown in Figure 6D. In this case, the light first passes through the SnS2. However, because of the wide bandgap, no diffraction ring is formed. As an RSA

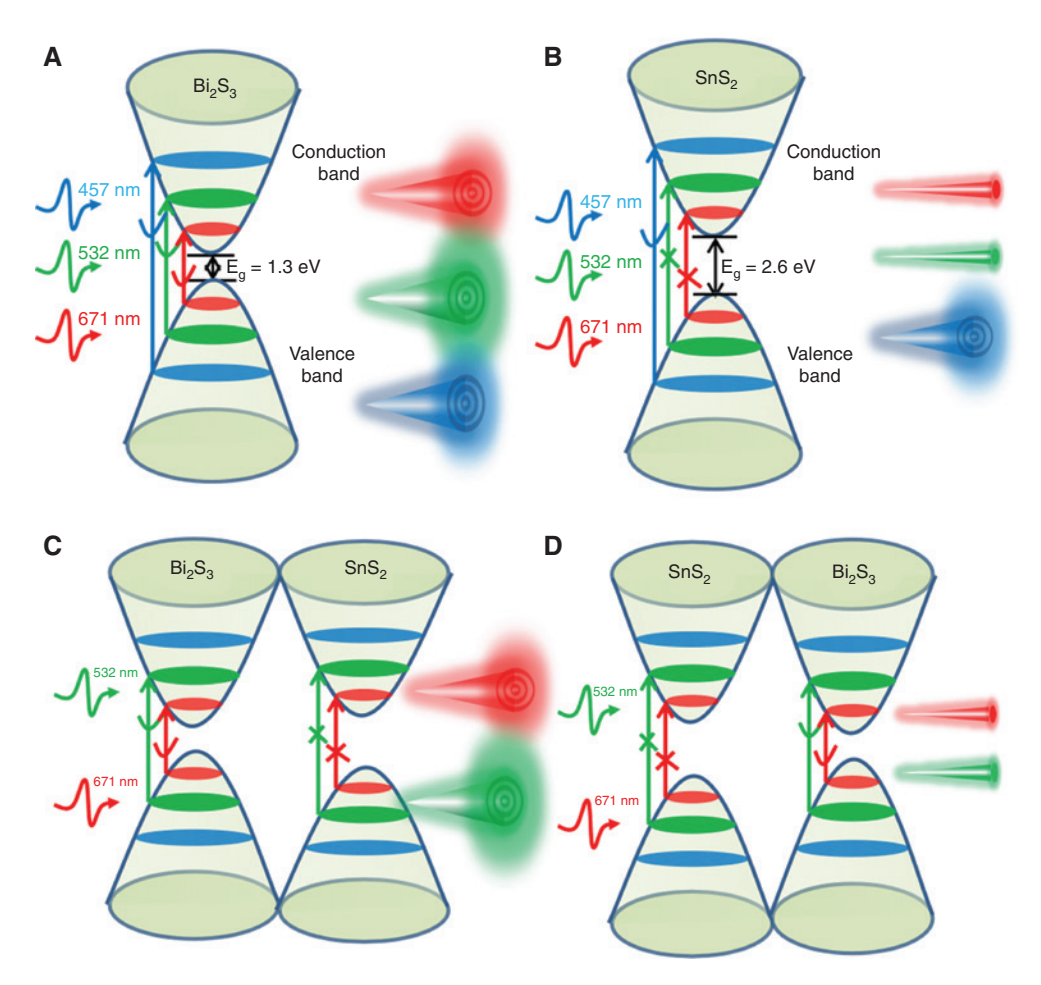


Figure 6: Microscopic principle of SSPM and all-optical diode. (A) The schematic diagram of SSPM based on Bi,S,; (B) the schematic diagram of SSPM based on SnS,; (C) positive propagation of light of all-optical diode; and (D) negative propagation of light of all-optical diode.

material, the SnS₂ greatly attenuates the power of the light passing through it, and thus, there is not enough energy to excite the nonlinear effect of subsequent 2D Bi₂S₂.

Figure 7 shows the scheme of the all-optical diode. The measured result is consistent with the simulated results shown in Figure 6. In this experiment, the blue CW laser with $\lambda = 457$ nm is used together with the green and red CW laser for comparison. Different from the red and green CW lasers that have a lower energy and can only pass the device in the positive devices, the blue CW laser can excite the nonlinear effect of the composite construction from both positive and reverse directions. Therefore, we take advantage of the wide bandgap and RSA property of SnS₂ to design a novel all-optical diode bases on the combined 2D Bi₂S₂/SnS₂ dispersions, which is similar to the traditional electronic diode. By using the proposed structure, the unidirectional propagation of light can be easily implemented.

3.5 The relationship between incident intensity and all-optical diode

Figure 8A shows the nonlinear effect when three different CW lights pass through the 2D Bi₂S₂ dispersions; as a result, all of them excite the diffraction ring. It means that the 2D Bi₂S₃ has excellent optical response to these CW lasers. Figure 8A uses the composite structure of 2D Bi₂S₂/SnS₂. Compared with Figure 8A, it is found that when light passes the diode from the positive direction,

some diffraction rings are darker than the light that only passes the 2D Bi₂S₃ dispersions. In contrast, when light passes the diode from the reverse direction, there is no diffraction ring generated. Especially, the blue CW laser with $\lambda = 457$ nm is able to excite the nonlinear effect from both positive and reverse directions of the optical diode. Figure 8B shows the experimental results where the triangle stands for the measured number of diffraction rings, and the fitted line is plotted based on the measured discrete data. It can be seen that the number of diffraction rings generated from the positive direction of the optical diode is more than that from the reverse direction when $\lambda = 457$ nm. This means that the 2D Bi₃S₃ has better optical response to incident light than SnS₂. The experimental results agree with the theoretical values obtained in previous sections.

4 Conclusions

The 2D materials present excellent application in optics. In this work, we have studied the properties of 2D Bi₂S₂ and SnS, dispersions with aspects of bandgap, absorption, and nonlinear optical effect. We measured the nonlinear refractive index of 2D Bi₂S₂ by SSPM and investigated the relationship between incident intensity and nonlinear optical effect, which help to design the novel all-optical device. On the basis of the bright and dark diffraction rings generated from the different laser power, we

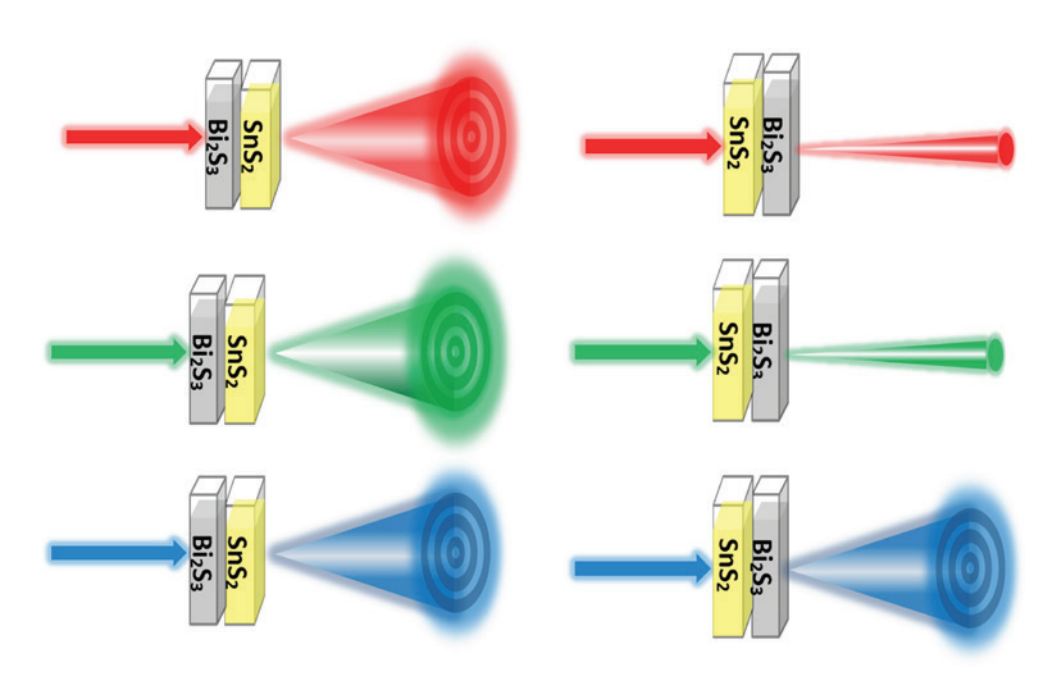


Figure 7: Experimental diagram of all-optical diode based on Bi₂S₃/SnS₂ with $\lambda = 457$ nm, $\lambda = 532$ nm, and $\lambda = 671$ nm.

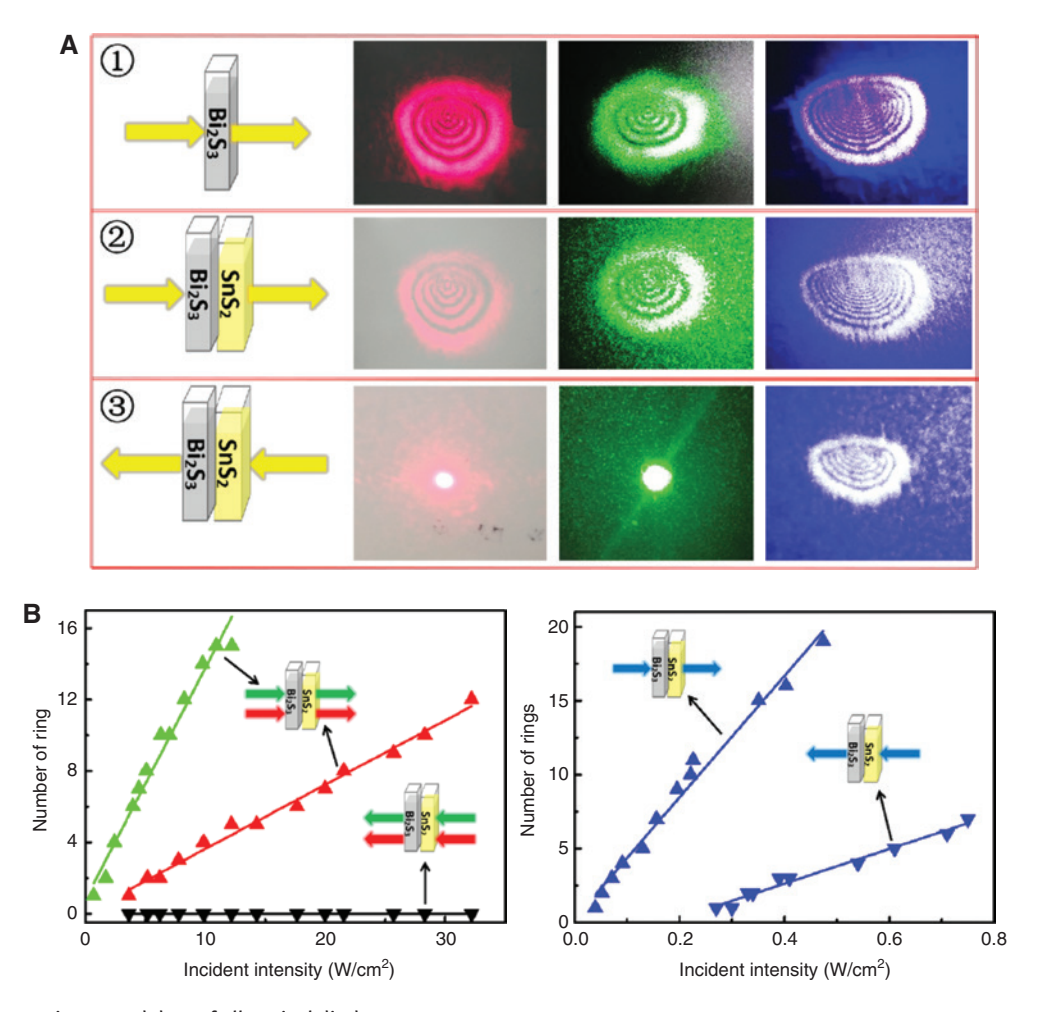


Figure 8: The experiment and data of all-optical diode. (A) Experiments of all-optical diode with a different range of wavelength; (B) the experimental data of diode with $\lambda = 532$ nm and $\lambda = 671$ nm, contrasting with $\lambda = 457$ nm based on the identical structure.

designed an all-optical switch by setting a threshold value of laser power of the diffraction ring. We have designed an all-optical diode with the combined structure (Bi₂S₂/SnS₂) by taking advantage of the RSA and wide bandgap properties of SnS₂. We also investigated the nonlinear optical responses of SnS₂ with different laser wavelengths, further illustrating the importance of bandgap in SSPM. The results from this work may have potential applications in the future design of nonreciprocal all-optical device.

Acknowledgments: This work is partially supported by the National Natural Science Foundation of China (grant nos. 11874269 and 61875133, Funder Id: http://dx.doi. org/10.13039/501100001809), the Science and Technology Project of Shenzhen (grant nos. JCYJ20180305125036005 and JCYJ20180305124842330, Funder Id: http://dx.doi. org/10.13039/501100013093), the Guangdong Natural Science Foundation (grant no. 2018A030313198, Funder Id: http://dx.doi.org/10.13039/501100003453), and the

China Postdoctoral Science Foundation (grant nos. 2017M622746 and 2018M633129, Funder Id: http://dx.doi. org/10.13039/501100010031).

Notes: The authors declare no competing financial interest.

References

- [1] Bao HF, Cui XQ, Li CM, Gan Y, Zhang J, Guo J. Photo switchable semiconductor bismuth sulfide (Bi,S,) nanowires and their selfsupported nanowire arrays. J Phys Chem C 2007;111:12279-83.
- [2] Tahir AA, Ehsan MA, Mazhar M. Photoelectrochemical and photo-responsive properties of Bi₂S₃ nanotube and nanoparticle thin films. Chem Mater 2010;22:5084-92.
- [3] Martinez L, Bernechea M, de Arquer FPG, Konstantatos G. Near IR-sensitive, non-toxic, polymer/nanocrystal solar cells employing Bi,S, as the electron acceptor. Adv Energy Mater 2011;1:1029-35.

- [4] Quan ZW, Yang J, Yang PP, Wang ZL, Li CX, Lin J. Facile synthesis and characterization of single crystalline Bi₂S₂ with various morphologies. Cryst Growth Des 2007;8:200-7.
- [5] Liu ZP, Xu D, Liang JB, Yu WC, Qian YT. Low-temperature synthesis and growth mechanism of uniform nanorods of bismuth sulfide. J Solid State Chem 2005;178:950-5.
- [6] Wang Y, Chen J, Peng W, et al. Syntheses, growth mechanism and optical properties of [001] growing Bi,S, nanorods. J Phys Chem C 2009:113:16009-14.
- [7] Konstantatos G, Levina L, Tang J, Sargent EH. Sensitive solution-processed Bi₂S₃ nanocrystalline photodetectors. Nano Lett 2008;8:4002-6.
- [8] Nair MTS, Nair PK. Photoconductive bismuth sulphide thin films by chemical deposition. Semicond Sci Tech 1990;5:1225.
- [9] Mane RS, Sankapal BR, Lokhande CD. Photoelectrochemical (PEC) characterization of chemically deposited Bi₂S₂ thin films from non-aqueous medium. Mater Chem Phys 1999;60:158-62.
- [10] Ghosh B, Kothiyal GP. Vapour phase growth of arsenic chalcogenide crystals and their characterization. Prog Cryst Growth Ch 1983:6:393.
- [11] Shah MP, Holmberg SH, Kostylev SA. Reversible switching in thin amorphous chalcogenide films - electronic effects. Phys Rev Lett 1973;31:542.
- [12] Wu LM, Dong YZ, Zhao JL, et al. Kerr nonlinearity in 2D graphdiyne for passive photonic diodes. Adv Mater 2019;31:1807981.
- [13] Loferski JJ. Theoretical considerations governing the choice of the optimum semiconductor for photovoltaic solar energy conversion. J Appl Phys 1956;27:777-84.
- [14] Du J, Tang PH, Liu JC, Zhao J. Broadband ultrafast spatial selfphase modulation for topological insulator Bi, Te, dispersions. Appl Phys Lett 2015;107:151101.
- [15] Li XH, Hu KH, Lyu B, et al. Enhanced nonlinear optical response of rectangular MoS₂ and MoS₂/TiO₂ in dispersion and film. J Phys Chem C 2016;120:18243-8.
- [16] Durbin SD, Arakelian SM, Shen YR. Laser-induced diffraction rings from a nematic-liquid-crystal film. Opt Lett 1981;6:411-3.
- [17] Zhang H, Virally S, Bao Q, et al. Z-scan measurement of the nonlinear refractive index of graphene. Opt Lett 2012;37:1856-8.
- [18] Wang GH, Zhang SF, Umran FA, et al. Tunable effective nonlinear refractive index of graphene dispersions during the distortion of spatial self-phase modulation. Appl Phys Lett 2014;104:141909.
- [19] Wang GZ, Zhang SF, Zhang XY, et al. Tunable nonlinear refractive index of two-dimensional MoS₂, WS₂, and MoSe₃ nanosheet dispersions. Photonics Res 2013;3:A51-5.
- [20] Zhang JD, Yu XF, Han WJ, et al. Broadband spatial self-phase modulation of black phosphorous. Opt Lett 2016;41:1704-7.
- [21] Shan YX, Wu LM, Liao YL, Tang J, Dai XY, Xiang YJ. A promising nonlinear optical material and its applications for all-optical switching and information converter based on the spatial selfphase modulation (SSPM) effect of TaSe, nanosheets. J Mater Chem C 2019;7:3811-6.
- [22] Wu LM, Xie ZJ, Lu L, et al. Few-layer tin sulfide: a promising black-phosphorus-analogue 2D material with exceptionally

- large nonlinear optical response, high stability, and applications in all-optical switching and wavelength conversion. Adv Opt Mater 2017;6:1700985.
- [23] Wu YL, Wu Q, Sun F, Cheng C, Meng S, Zhao JM. Emergence of electron coherence and two-color all-optical switching in MoS, based on spatial self-phase modulation. Proc Natl Acda Sci USA 2015;112:11800-5.
- [24] Lu L, Wang WH, Wu LM, et al. All-optical switching of two continuous waves in few layer bismuthene based on spatial cross-phase modulation. ACS Photonics 2017;4:2852-61.
- [25] Shapiro JH, Razavi M. Continuous-time cross-phase modulation and quantum computation. New J Phys 2007;9:16.
- [26] Shen Y, Watanabe T, Arena DA, et al. Nonlinear cross-phase modulation with intense single-cycle terahertz pulses. Phys Rev Lett 2007:99:043901.
- [27] Wu YF, Keller BP, Keller S, et al. Very high breakdown voltage and large transconductance realized on GaN heterojunction field effect transistors. Appl Phys Lett 1996;69:1438-40.
- [28] Dong YC, Chertopalov S, Maleski K, et al. Saturable absorption in 2D Ti₂C₂ MXene thin films for passive photonic diodes. Adv Mater 2018;30:1705714.
- [29] Xu Y, Schoonen MAA. The absolute energy positions of conduction and valence bands of selected semiconducting minerals. Am Mineral 2000;85:543-56.
- [30] Lawaetz P. Valence-band parameters in cubic semiconductors. Phys Rev B 1971;4:3460.
- [31] Guo SQ, Jing TZ, Zhang X, et al. Mesoporous Bi₂S₃ nanorods with graphene-assistance as low-cost counter-electrode materials in dye-sensitized solar cells. Nanoscale 2014;6:14433-40.
- [32] Ai KL, Liu YL, Liu JH, Yuan QH, He YY, Lu LH. Large-scale synthesis of Bi₂S₂ nanodots as a contrast agent for in vivo X-ray computed tomography imaging. Adv Mater 2011;23:4886-91.
- [33] Chen GY, Yu YQ, Zheng K, et al. Fabrication of ultrathin Bi₂S₂ nanosheets for high-performance, flexible, visible-NIR photodetectors. Small 2015;11:2848-55.
- [34] Huang WC, Xing CY, Wang YZ, et al. Facile fabrication and characterization of two-dimensional bismuth(III) sulfide nanosheets for high-performance photodetector applications under ambient conditions. Nanoscale 2018;10:2404-12.
- [35] Weng B, Zhang X, Zhang N, Tang ZR, Xu YJ. Two-dimensional MoS, nanosheet-coated Bi,S, discoids: synthesis, formation mechanism and photocatalytic application. Langmuir 2015;31:4314-22.
- [36] Bernechea M, Cao YN, Konstantatos G. Size and bandgap tunability in Bi₂S₂ colloidal nanocrystals and its effect in solution processed solar cells. J Mater Chem A 2015;3:20642-8.
- [37] Trentelman K. A note on the characterization of bismuth black by Raman microspectroscopy. J Raman Spectrosc 2009;40:585-9.
- [38] Sun ZB, Xie HH, Tang SY, et al. Ultrasmall black phosphorus quantum dots: synthesis and use as photothermal agents. Angew Chem Int Ed 2015;54:11526-30.
- [39] Huang WC, Jiang XT, Wang YZ, et al. Two-dimensional beta-lead oxide quantum dots. Nanoscale 2018;10:20540-7.